Taichunins E−T, Isopimarane and a 20-*nor*-Isopimarane Diterpene, from *Aspergillus taichungensis* (IBT 19404): Structures and Inhibitory Effects on RANKL-Induced Formation of Multinuclear Osteoclasts

Ahmed H. H. El-Desoky,[†, ‡,○] Natsumi Inada,[†,○] Yuka Maeyama,[†,○] Hikaru Kato,[†] Yuki Hitora,[†] Momona Sebe,[†] Mika Nagaki,[†] Aika Kai,[†] Keisuke Eguchi,[†] Tomoaki Inazumi,[§] Yukihiko Sugimoto,[§] Jens C. Frisvad,[⊥] Robert M. Williams,[▽] Sachiko Tsukamoto[†,*]

[†] Department of Natural Medicines, Graduate School of Pharmaceutical Sciences, Kumamoto University, 5-1 Oe-honmachi, Kumamoto 862-0973, Japan

[‡] Pharmaceutical Industries Research Division, Pharmacognosy Department, National Research Centre, 33 El Bohouth St. (Former El Tahrir St.), Dokki, P.O. 12622, Giza, Egypt

[§] Department of Pharmaceutical Biochemistry, Graduate School of Pharmaceutical Sciences, Kumamoto University, 5-1 Oe-honmachi, Kumamoto 862-0973, Japan

[⊥] Section for Synthetic Biology, Department of Biotechnology and Biomedicine, Soltofts Plads Building 221, Technical University of Denmark, 2800 Kongens Lyngby, Denmark

[▽] Department of Chemistry, Colorado State University, 1301 Center Avenue, Fort Collins, CO 80523, USA

[○] These authors contributed equally.

* Corresponding author.

E-mail address: sachiko@kumamoto-u.ac.jp

Fifteen new isopimarane-type diterpenes, taichunins E–S (**1–15**), and a new 20-*nor*-isopimarane, taichunin T (**16**), together with four known compounds were isolated from *Aspergillus taichungensis* (IBT 19404). The structures of these new compounds were determined by NMR and mass spectroscopy, and their absolute configurations were analyzed by NOESY and TDDFT calculations of ECD spectra. Taichunins G, K, and N (**3**, **7**, and **10**) completely inhibited the receptor activator of nuclear factor-κB ligand (RANKL)-induced formation of multinuclear osteoclasts in RAW264 cells at 5 μM, with **3** showing 92% inhibition at a concentration of 0.2 μM.

An imbalance in bone remodeling owing to disorders of bone formation by osteoblasts and resorption by osteoclasts causes skeletal diseases such as osteoporosis, periodontal disease, and rheumatoid arthritis.[1–3] For elderly people, osteoporotic fractures are life-threatening events; the development of therapeutic agents to treat osteoporosis is therefore of great importance.[4] Osteoclasts differentiate from a monocyte/macrophage lineage by stimulation with receptor activator of nuclear factor-κB ligand (RANKL). RANKL activates several downstream signaling pathways such as the NF-κB and MAPK signaling pathways, which subsequently induce the expression of osteoclast-specific genes including those encoding tartrate-resistant acid phosphatase (TRAP) and several enzymes involved in cell fusion, leading to development of mature osteoclasts.

Inhibitors of RANKL-induced formation of multinuclear osteoclasts are seen as promising drug leads in the prevention and treatment of osteoporosis. We screened extracts of marine sponges and fungi by measuring the RANKL-induced upregulation of TRAP activity in RAW264 cells, and found several inhibitors from marine sponges[5–8] and a fungus.[9] Halenaquinone, a pentacyclic polyketide, from the marine sponge *Petrosia alfani* inhibited RANKL-induced osteoclastogenesis with an IC_{50} value of 2 μM, which is at least resulted by suppressing the NF-κB and Akt signaling pathways through inhibition of IκB degradation and Akt phosphorylation, respectively.[5] Ceylonamides A–F[6] and ceylonins A–F,[7] spongian diterpenes, were isolated from the marine sponge *Spongia ceylonensis*, and showed the inhibition of RANKL-induced osteoclastogenesis in RAW264 macrophages without toxicity. Sipholane type triterpenes, isolated from the Red Sea marine sponge *Siphonochalina siphonella*, inhibited RANKL-induced osteoclastogenesis.[8] A series of enantiomeric prenylated indole alkaloids were isolated from the marine-derived *Aspergillus protuberus* MF297-2[10] and the terrestrial *A.*

amoenus NRRL 35600,[11] and (−)-enantiomers of notoamides A and B, 6-*epi*-notoamide T, and stephacidin A inhibited RANKL-induced osteoclastogenesis more potently than their respective (+)-enantiomers.[9] Among these, (−)-6-*epi*-notoamide T was the most potent inhibitor with an IC_{50} value of 1.7 μM.

Terpenes are an extensive group of natural products from plants, fungi, and marine organisms, with diverse structures and interesting biological activities.[12] The pimarane/isopimarane diterpenes are a subgroup of the diterpenes with cytotoxic, antimicrobial, antiviral, and phytotoxic activities. Among them, sphaeropsidin A[13] was isolated from *Sphaeropsis sapinea* f. sp. *cupressi* and *Diplodia mutila* as a phytotoxin, and subsequently, sphaeropsidins B and C were also isolated from the same fungus.[14] During a search for biologically interesting prenylated indole alkaloids from the genera *Aspergillus*,[10,11,15,16] we isolated four new *nor*-isopimarane diterpenes, taichunins A−D from *A. taichungensis* (IBT 19404).[17] In our screening program for biologically active metabolites, the fractions of this fungal culture inhibited RANKL-induced formation of multinuclear osteoclasts in murine RAW264 cells. Here, we report the structures of 15 new isopimaranes (**1**–**15**) and a new 20-*nor*-isopimarane (**16**) from *A. taichungensis* (IBT 19404) and their bioactivities.

RESULTS AND DISCUSSION

Isolation and Structural Elucidation of New Compounds (1–16). The *n*-BuOH extract from a rice culture of *A. taichungensis* (IBT 19404) was partitioned between *n*-BuOH and water. The *n*-BuOH-soluble fraction was dissolved in 90% MeOH−H_2O and extracted by *n*-hexane, followed by further fractionation by ODS and silica gel column chromatography as well as HPLC to afford 15 new isopimarane-type diterpenes, taichunins E−S (**1**−**15**), and a new 20-*nor*-isopimarane, taichunin T (**16**), along with known compounds sphaeropsidin B[14] (**17**), aspergiloids C and D[18] (**18** and **19**), and 1β,7α-dihydroxysandaracopimar-8(14),15-diene[19] (**20**).

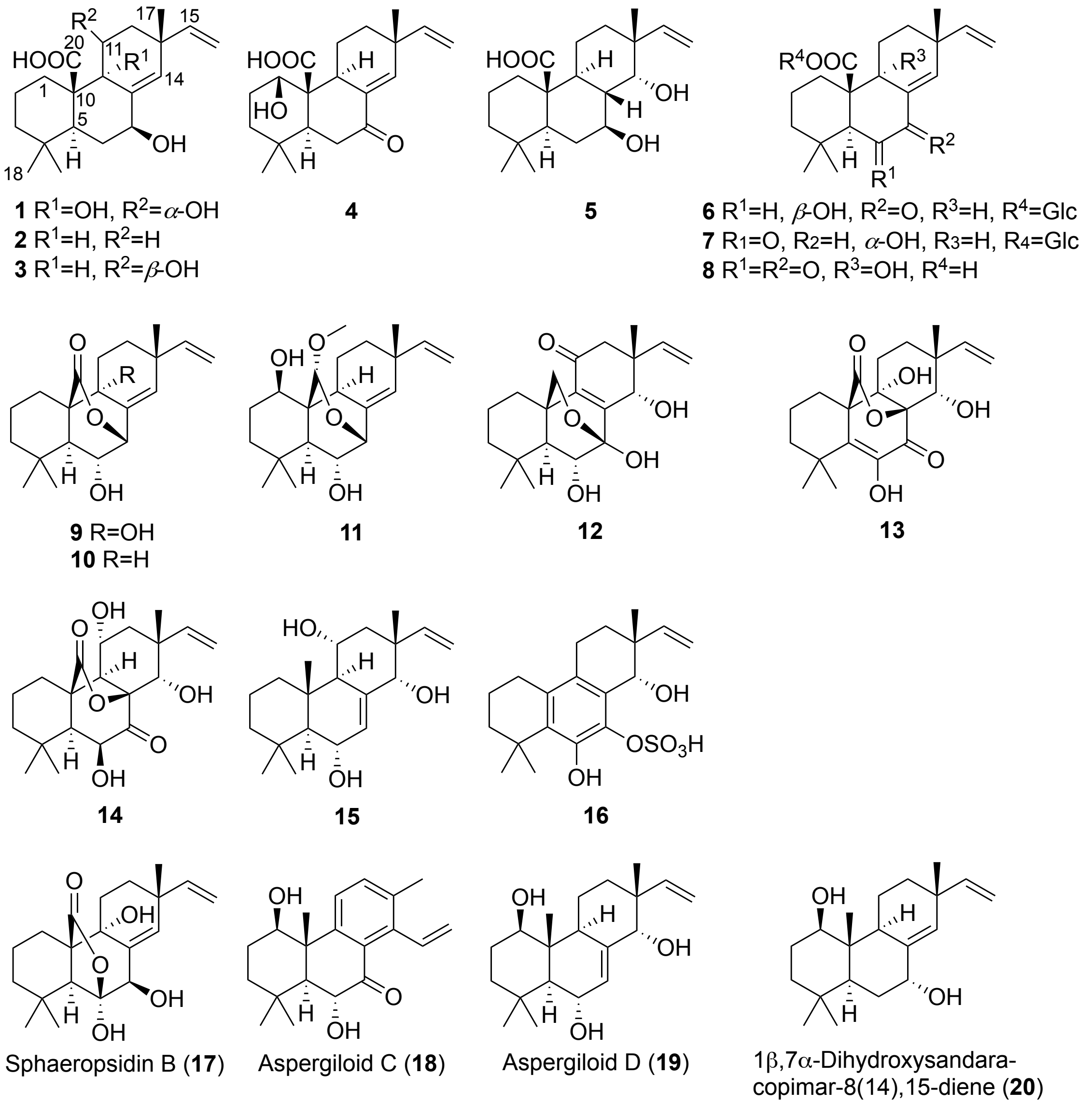

Taichunin E (**1**) has the molecular formula $C_{20}H_{30}O_5$, which was determined by HRESIMS. The ^1H and ^{13}C NMR spectra of **1** (Table 1) showed three singlet methyls [δ_H 0.93 (s), δ_C 24.6 (C-17); δ_H 0.86 (s), δ_C 32.5 (C-18); δ_H 0.70 (s), δ_C 20.4 (C-19)], a monosubstituted alkene [δ_H 5.79 (dd, J = 17.5, 10.5 Hz), δ_C 148.6 (C-15); δ_H 4.87 (d, J =

10.5) and 4.93, (d, J = 17.5 Hz), δ_C 109.9 (C-16)], a trisubstituted alkene [δ_H 5.51 (s), δ_C 124.9 (C-14); δ_C 140.3 (C-8)], a methine [δ_H 1.78 (m), δ_C 45.0 (C-5)], two oxygenated methines [δ_H 4.19 (brs), δ_C 67.5 (C-7); δ_H 3.87 (d, J = 9.5 Hz), δ_C 66.1 (C-11)], five methylenes [δ_H 1.28−2.37 (10H)], three quaternary carbons [δ_C 33.5 (C-4); 56.0 (C-10); 37.5 (C-13)], and a carbonyl carbon [δ_C 175.9 (C-20)]. The molecular formula is consistent with six degrees of unsaturation; three of them accounting for the carbonyl group (C-20) and double bonds $\Delta^{8(14)}$ and Δ^{15} and the remaining three indicating the presence of three rings. The presence of three singlet methyls and the monosubstituted and trisubstituted alkenes is reminiscent of a tricyclic diterpene structure such as a pimarane or isopimarane diterpene. COSY correlations established three spin systems, H_2-1/H_2-2/H_2-3, H-5/H_2-6/H-7/7-OH, 11-OH/H-11/H_2-12, and H-15/H-16, along with weak long-range COSY correlations H-14/H-7 and H-14/H_2-12 (Figure 1A). HMBCs from H_3-18 and H_3-19 to C-3, C-4, and C-5 and from H_3-19 to C-18 suggest that C-4 is substituted by two methyl groups. HMBCs from H_2-1 and H-5 to C-10 and C-20 showed substructure ***a*** (Figure 1A). HMBCs from H-15 and H_3-17 to C-12, C-13, and C-14 and from H_3-17 to C-15 implied that quaternary carbon C-13 is substituted by singlet methyl and vinyl groups. HMBCs from H_2-12 and H-14 to the oxygenated carbon C-9 (δ_C 73.6) and from 9-OH (δ_H 4.19) to another oxygenated carbon C-11 indicated substructure ***b*** (Figure 1A). The connections C-7/C-8 and C-9/C-10 were indicated by HMBCs from H-7 to C-9, from 7-OH to C-8, and from 9-OH to C-10. NOE correlations H-11/H_3-17 and H-11/H-1β implied β-orientations of H-1β, H-11, and H_3-17 (Figure 1B). NOE correlations, H-1α/H-5, H-6α/H_3-18, and H-6β/H_3-19, confirmed α-orientations of H-1α, H-5, H-6α, and H_3-18 and β-orientations of H-6β and H_3-19. Meanwhile, correlations H-1α/9-OH and H-1α/H-5 showed the axial β-orientation of the carboxylic acid (C-20) and axial α-orientations of 9-OH and H-5, while correlation 7-OH/H-14 showed the β-orientation of 7-OH. These data revealed the relative configuration of **1**. The absolute configuration of **1** was elucidated by ECD, with the calculated spectrum of configuration 5*S*,7*S*,9*R*,10*R*,11*R*,13*R* matching the experimental spectrum with the positive Cotton effect around 220 nm and negative ellipticity in the short-wavelength side (Figure 1C). Thus, the absolute configuration of **1** was determined as shown.

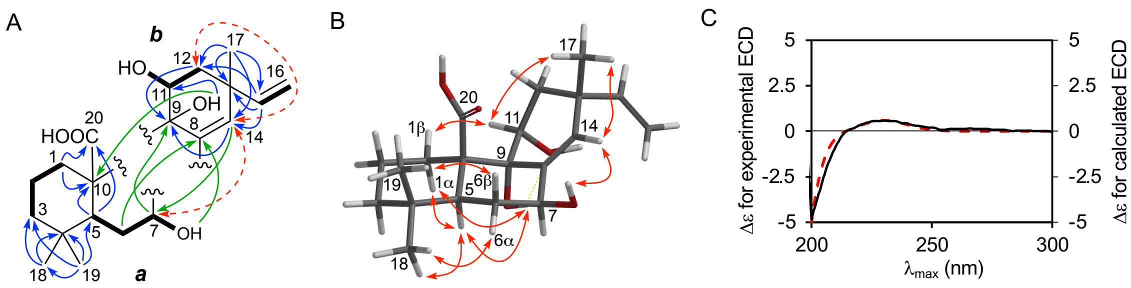

Figure 1. (A) COSY (bold lines) and long-range COSY (red dotted arrows) correlations and key HMBCs (blue and green arrows) for substructures ***a*** and ***b*** in **1**. (B) Key NOEs for **1**. (C) Experimental ECD spectrum of **1** (black solid line) and calculated ECD spectrum of 5*S*,7*S*,9*R*,10*R*,11*R*,13*R*-**1** (dashed red line).

Table 1. NMR Data of **1** (DMSO-d_6)

no.	δ_C, mult.	δ_H, mult., (*J* in Hz)	HMBC
1	29.5, CH_2	α 1.29, m	10, 20
		β 2.37, d (13.2)	
2	19.8, CH_2	α 1.38, m	2, 4, 5, 10
		β 1.73, m	
3	41.6, CH_2	α 1.14, m	4, 19
		β 1.28, m	
4	33.5, C		
5	45.0, CH	1.78, m	4, 6, 10, 19, 20

6	31.8, CH_2	α 2.04, d (11.7)	5, 7, 8
		β 1.76, m	5, 7
7	67.5, CH	4.19, m	6, 8, 9
8	140.3, C		
9	73.6, C		
10	56.0, C		
11	66.1, CH	3.87, d (9.5)	
12	40.8, CH_2	α 1.41, m	9, 11, 13, 14
		β 1.39, m	9, 11, 13, 14, 15, 17
13	37.5, C		
14	124.9, CH	5.51, brs	8, 9, 11, 12, 13, 15
15	148.6, CH	5.79, dd (17.5, 10.5)	12, 13, 14, 17
16	109.9, CH_2	a 4.93, d (17.5)	13, 15
		b 4.87, d (10.5)	13, 15
17	24.6, CH_3	0.93, s	12, 13, 14, 15
18	32.5, CH_3	0.86, s	3, 4, 5, 19
19	20.4, CH_3	0.70, s	3, 4, 5, 18
20	175.9, C		
7-OH		4.64, d (4.7)	6, 7, 8
9-OH		4.19, s	8, 10, 11
11-OH		4.79, s	
20-OH		12.1, brs	

The molecular formulas of taichunins F (**2**) ($C_{20}H_{30}O_3$) and G (**3**) ($C_{20}H_{30}O_4$) contain two and one fewer oxygen atoms than that of **1**, respectively. The NMR spectra of **2** (Tables S1) are almost superimposable on those of **1** except for the absence of two oxygenated methine and non-protonated carbons and the presence of additional methylene (C-11) and methine (C-9) groups, indicating that two hydroxy groups in **1** are replaced with two hydrogens in **2**. The COSY correlations and HMBCs (Figure 2A) confirmed the planar structure of **2**, and the relative configuration was assigned by NOE correlations (Figure 2B). The ^{1}H NMR spectrum of **3** (Tables S2) showed an additional oxygenated methine (C-11) instead of the methylene in **2**, which was substantiated by the COSY correlations and HMBCs (Figure 2A). NOE correlations revealed β-orientations of 11-OH and 7-OH (Figure 2B). The ECD spectra of **2** and **3** showed similar patterns to that of **1** (Figure 2C), indicating the same absolute configurations for **1**−**3**.

Taichunin H (**4**) has the molecular formula $C_{20}H_{28}O_4$, with two fewer hydrogens than that of **3**. The NMR data (Table S3) showed that the position of the hydroxy group at C-11 in **3** is changed to C-1 in **4**, and that the hydroxy methine of **3** is replaced with a ketone carbon (δ_C 197.5) in **4**, which was supported by the COSY and HMBC data (Figure 2A). The β-orientation of 1-OH was indicated by the NOE correlation (Figure 2B). Signs of peaks around 230 and 250 nm in the calculated ECD spectrum of 1*R*,5*S*,9*S*,10*R*,13*R*-**4** confirmed the absolute configuration of **4** (Figure 2C).

Taichunin I (**5**) has the molecular formula $C_{20}H_{32}O_4$, with one more H_2O unit than that of **2**. The NMR spectra of **5** (Table S4) are almost superimposable on those of **2** except for the disappearance of the double bond $\Delta^{8(14)}$ of **2** and appearance of two methines (C-8 and C-14), suggesting the addition of a H_2O unit to the double bond (Figure 2A). The α-orientated 14-OH was consistent with the NOE correlations (Figure 2B). The absolute configuration of **5** was determined by the calculated ECD of configuration 5*S*,7*S*,8*S*,9*S*,10*S*,13*R*,14*R*, which matched the experimental ECD spectrum (Figure 2C).

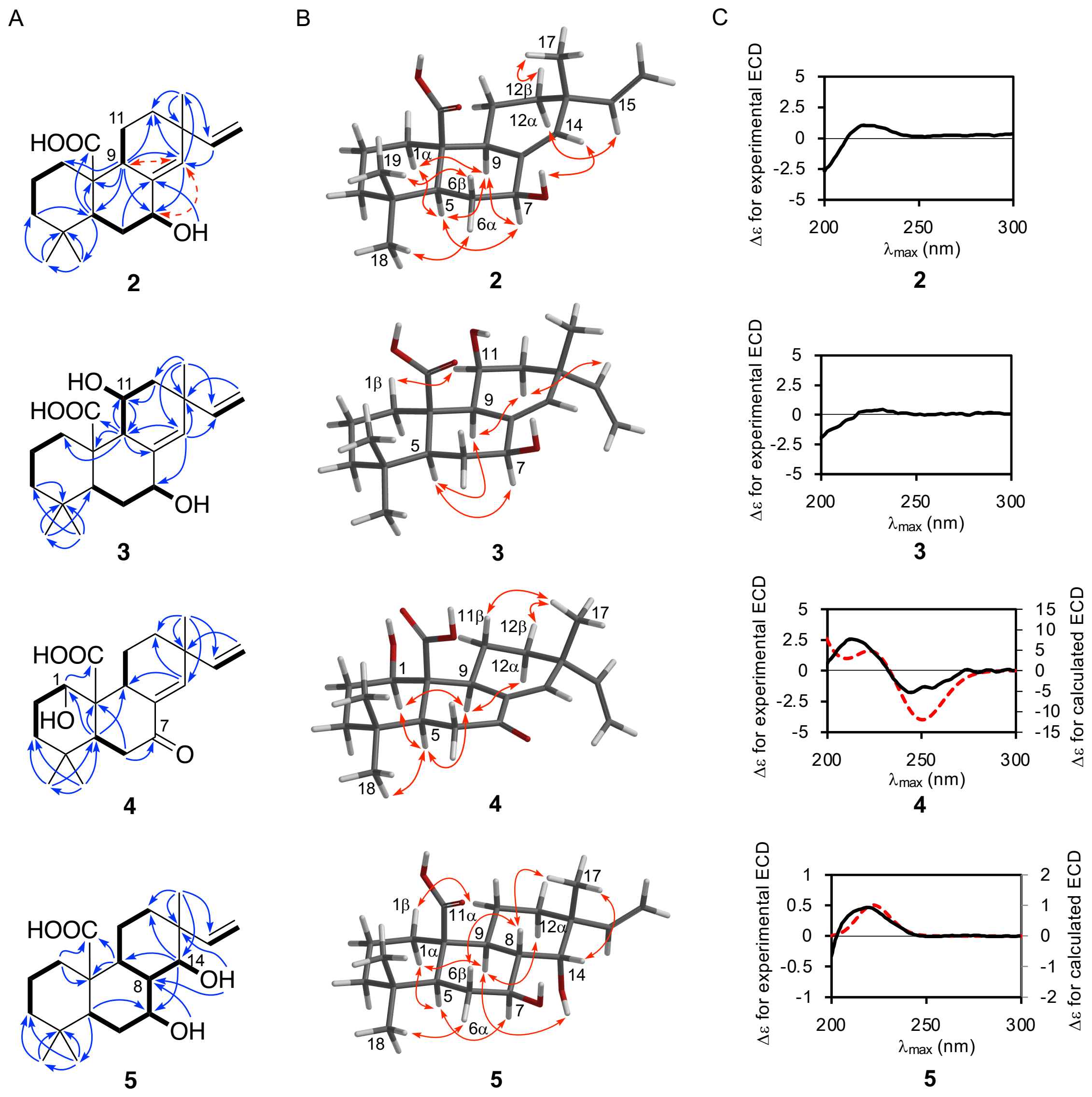

Figure 2. (A) COSY (bold lines) and long-range COSY (red dotted arrows) correlations and key HMBCs (blue arrows) for **2**–**5**. (B) Key NOEs for **2**–**5**. (C) Experimental ECD spectra of **2**–**5** (black solid line) and calculated ECD spectra of 1*R*,5*S*,9*S*,10*R*,13*R*-**4** and 5*S*,7*S*,8*S*,9*S*,10*S*,13*R*,14*R*-**5** (dashed red line).

Taichunins J (**6**) and K (**7**) possess identical molecular formulas $C_{26}H_{38}O_9$, which is a $C_6H_{10}O_5$ unit more than that of **4**. The NMR data (Table S5) of **6** indicated the presence of a hexose unit with signals δ_H 3−5.3 and δ_C 60−95, and axial-axial coupling constants

(J = 8−9 Hz) observed for H-1'/H-2'/H-3'/H-4'/H-5' showed that it is a β-linked glucose. The HMBC correlation from H-1' to C-20 suggests that the glucose moiety is attached to the C-20 position (Figure 3A). The glucose liberated from **6** by acid hydrolysis was assigned to the D-series by HPLC analysis after derivatization.[20] COSY and HMBC correlations revealed a hydroxy group attached to C-6 instead of C-1 in **4** (Figure 3A). The magnitude of the coupling constant (J = 7.7 Hz) between axially-oriented H-5 and H-6 implied that H-6 is in a pseudoequatorial orientation and that 6-OH is pseudoaxially β-oriented (Figure 3B). The ECD pattern of **6** was the same as **4**, thus indicating a 5*S*,6*S*,9*S*,10*S*,13*R* configuration for **6** (Figure 3C). The NMR spectra (DMSO-d_6) of **7** (Table S6) were almost identical to those of **6**, and HMBCs confirmed the presence of a ketone at C-6 and an oxygenated methine at C-7 (Figure 3A). Since the ^{1}H-^{1}H coupling constants of the sugar moiety were not clearly observed in DMSO-d_6, the pentaacetate derivative (**7a**) was prepared. Analysis of the ^{1}H NMR spectrum of **7a** confirmed the presence of a β-linked glucose moiety. The relative and absolute configurations of **7** were determined in the same way as for **6** (Figures 3B and C).

Taichunin L (**8**) has the molecular formula $C_{20}H_{26}O_5$, indicating six degrees of unsaturation and one more oxygen than that of the aglycone moiety of **6**. Analysis of the 2D NMR spectra in pyridine-d_5 (Table S7) showed the presence of a hydroxy group at C-9 (δ_C 71.2) and a ketone at C-7 (δ_C 192.6) (Figure 3A). From the molecular formula, an additional ketone was suggested to be located at C-6, but its ^{13}C signal and HMBCs were not detected. To confirm the structure of **8**, it was reduced by sodium borohydride and HMBC correlations of the product (**8a**) (Table S8, Figure 3A) clearly indicated the presence of a ketone at C-6 (δ_C 205.6) and an oxygenated methine at C-7 (δ_C 74.3). The relative configuration of **8** was deduced from NOE data (Figure 3B), and the calculated

ECD peaks at 208, 242, and 272 nm matched those of 5*R*,9*R*,10*R*,13*R*-**8** (Figure 3C). Thus, the absolute configuration of **8** was established.

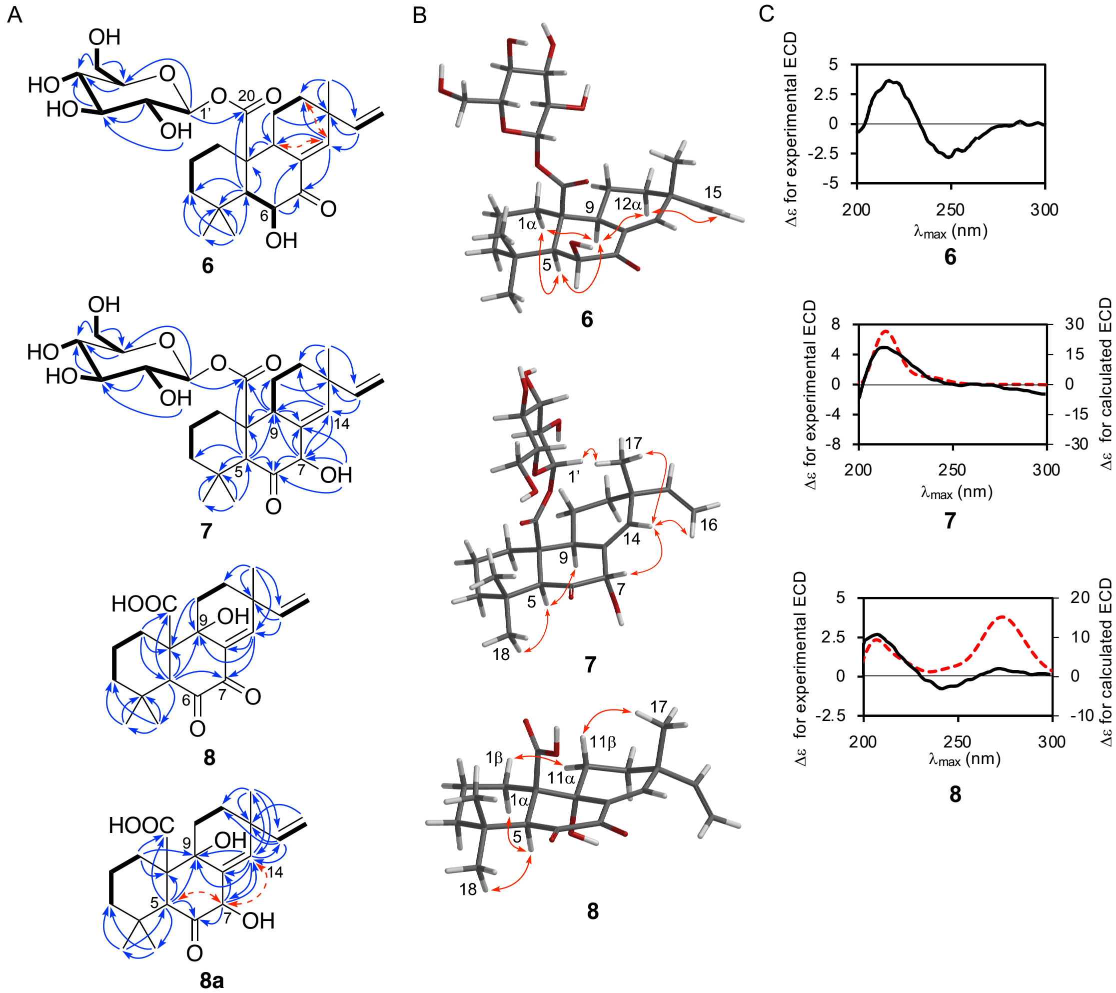

Figure 3. (A) COSY (bold lines) and long-range COSY (red dotted arrows) correlations and key HMBCs (blue arrows) for **6**−**8** and **8a**. (B) Key NOEs for **6**−**8**. (C) Experimental ECD spectra of **6**−**8** (black solid line) and calculated ECD spectra of the aglycone moiety of 5*S*,7*S*,9*S*,10*S*,13*R*-**7** and 5 *R*,9*R*,10*R*,13*R*-**8** (dashed red line).

Taichunin M (**9**) has the molecular formula $C_{20}H_{28}O_4$, suggesting seven degrees of unsaturation. Analysis of the 2D NMR spectra (Table S9) showed that **9** comprises a carbonyl carbon at C-20, hydroxy groups at C-6 and C-9, and $\Delta^{8(14)}$ and Δ^{15} double bonds. The HMBC from H-7 to C-20 suggested that **9** has an ester linkage between C-7 and C-20 to form a δ-lactone ring (Figure 4A). NOE correlations revealed the α-orientations of 6-OH and 9-OH and β-orientation of the δ-lactone ring (Figure 4B). The absolute configuration of **9** was determined by the calculated ECD spectrum (Figure 4C).

Taichunin N (**10**) has the molecular formula $C_{20}H_{28}O_3$, with one fewer oxygen atom than that of **9**. ^{1}H and ^{13}C NMR spectra of **10** (Table S10 and Figure 2) revealed that an oxygenated non-protonated carbon at C-9 of **9** was replaced with a methine [δ_H 2.17 (ddd, J = 11.6, 3.8, 3.0 Hz), δ_C 46.1], suggesting the loss of 9-OH of **9**. The structure was supported by a HMBC from H-7 and H-14 to C-9 (Figure 4A). NOE and ECD spectra (Figures 4A and 4B) showed the absolute configuration of **10**.

The molecular formula of taichunin O (**11**) was determined to be $C_{21}H_{32}O_4$ by HRESIMS, which is a CH_4 unit more than that of **9**. The 2D NMR spectra (Table S11, Figure 4A) showed the presence of a hydroxy group at C-1 and a methoxyl group at C-20 instead of the carbonyl oxygens in **9** and **10**. NOE correlations revealed that H-20 is on the β-face with the *R**-configuration along with the axial α-orientations of H-1, H-5, and H-9 (Figure 4B). The absolute configuration of **11** was determined by the calculated ECD spectrum (Figure 4C).

Taichunin P (**12**) has the molecular formula $C_{20}H_{28}O_5$, which is one oxygen atom more than that of **9**. Analysis of the 2D NMR data (Table S12, Figure 4A) indicated that the δ-lactone of **9** is changed to a tetrahydropyran in **12**. Additionally, the presence of a ketone [δ_C 195.6 (C-20)], a tetrasubstituted double bond [δ_C 154.2 (C-8) and 138.8 (C-9)], and three hydroxy groups at C-6, C-7, and C-14 were revealed. The relative and absolute configurations were elucidated by NOE (Figure 4B) and ECD experiments

(Figure 4C).

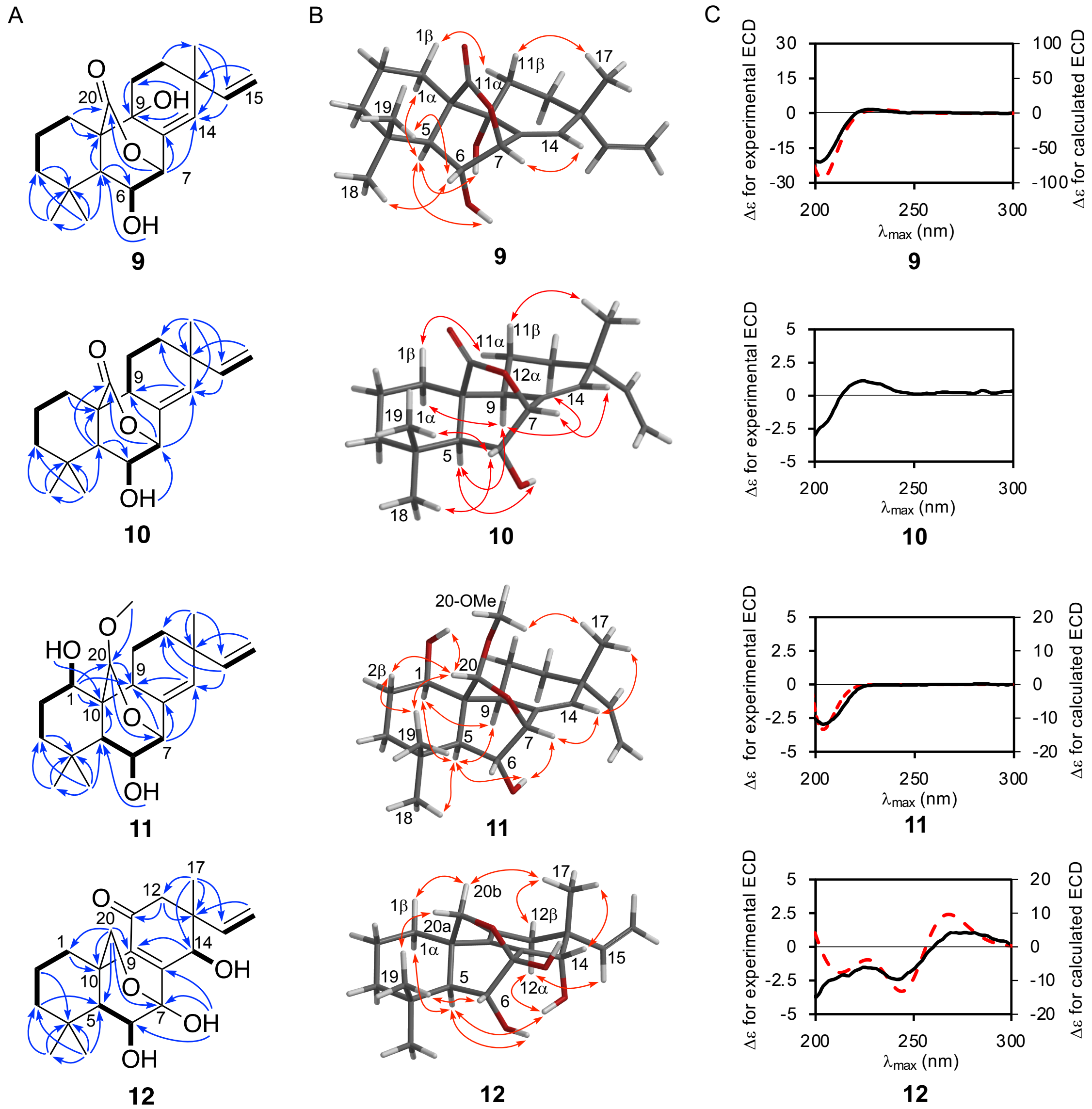

Figure 4. (A) COSY correlations (bold lines) and key HMBCs (arrows) for **9**–**12**. (B) Key NOEs for **9**–**12**. (C) Experimental ECD spectra of **9**–**12** (black solid line) and calculated ECD spectra of 5*S*,6*R*,7*R*,9*R*,10*R*,13*R*-**9**, 1*R*,5*S*,6*R*,7*R*,9*S*,10*S*,13*R*,20*R*-**11**, and 5*S*,6*R*,7*R*,9*S*,10*R*,13*R*,14*S*-**12** (dashed red line).

Taichunin Q (**13**) has the molecular formula $C_{20}H_{26}O_6$, implying eight degrees of unsaturation. The NMR spectra (Table S13) indicated that **13** has a structure analogous to **9** and **10**. The 2D NMR data suggested that carbons C-8 (δ_C 82.8), C-9 (δ_C 81.7), and C-14 (δ_C 68.5) are oxygenated (Figure 5A), and COSY correlation of H-14/14-OH clearly showed the presence of a hydroxy group at C-14. Analysis of HMBCs indicated that **13** possesses carbonyl carbons at C-20 (δ_C 176.0) and C-7 (δ_C 187.7). HMBCs from H_2-1 and H_3-19 to an olefine carbon C-5 (δ_C 130.3) indicated that C-6 is a hydroxy olefine carbon [δ_H 8.68 (s, 6-OH), δ_C 144.8]. Although no HMBC was observed for C-6, this is supported by its ^{13}C chemical shift and molecular formula. From the remaining hydrogen atom in the formula, a lactone was predicted to form between the carbonyl carbon at C-20 and oxygen atom at C-8 or C-9. NOE correlations (Figure 5B) showed that the oxygen atoms at C-8 and C-9 are β- and α-oriented, respectively, and a γ-lactone is thus formed with the oxygen at C-8 in the β-face. Signs of peaks in the calculated ECD data revealed the absolute configuration of **13** (Figure 5C).

Taichunin R (**14**) has the molecular formula $C_{20}H_{28}O_6$, which is two mass units more than that of **13**. The NMR spectra (Table S14) resemble those of **13** except for the absence of the $\Delta^{5(6)}$ double bond, the presence of two methines (C-5 and C-6), and the positions of hydroxy groups at C-6 and C-11 (Figure 5A). The relative and absolute configurations of **14** were determined from NOE (Figure 5B) and calculated ECD (Figure 5C) data.

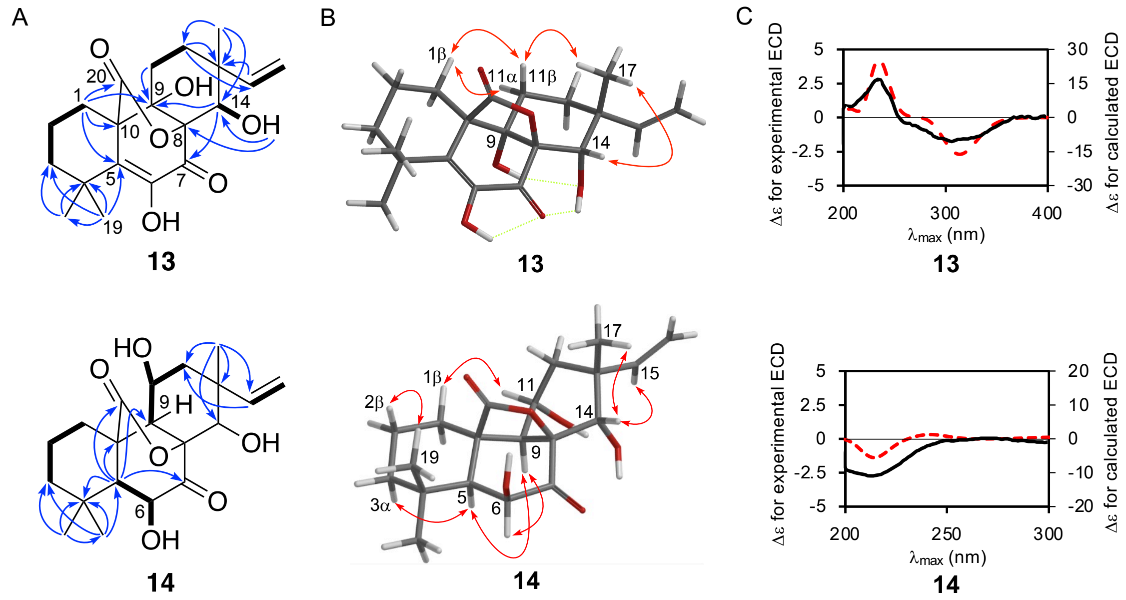

Figure 5. (A) COSY correlations (bold lines) and key HMBCs (arrows) for **13** and **14**. (B) Key NOEs for **13** and **14**. (C) Experimental ECD spectra of **13** and **14** (black solid line) and calculated ECD spectra of 8*R*,9*S*,10*R*,13*R*,14*S*-**13** and 5*S*,6*S*,8*S*,9*S*,10*R*,11*R*,13*R*,14*R*-**14** (dashed red line).

Taichunin S (**15**) has the molecular formula $C_{20}H_{32}O_3$, which is the same as that of aspergiloid D[18] (**19**), and the NMR spectra of **15** (Table S15) resembled those of **19**. Analysis of the 2D NMR spectra of **15** (Figure 6A) indicated the presence of a hydroxy group at C-11 [δ_H 3.56 (m), δ_C 65.9] instead of C-1 in **19**. NOE correlations showed the relative configuration of **15** (Figure 6B), and, due to its weak Cotton effect, the absolute configuration was deduced from the biogenetic relationships with **1**−**14**.

Taichunin U (**16**) has the molecular formula $C_{19}H_{26}O_6S$, with the presence of a sulfate moiety. The ^{1}H and ^{13}C NMR spectra (Table S16) of **16** were very similar to those of diplopimarane,[21] and analysis of the 2D NMR spectra indicated substructures ***a*** and ***b***

(Figure 6A). HMBCs established the carbon framework and positions of hydroxy groups at C-6 and C-14, indicating the position of the sulfate to be at C-7. The NOE correlation H-14/H_3-17 showed the relative configuration of 13*R**,14*S** (Figure 6B). Although **16** showed no ECD peak, the positive sign of the specific rotations of **16** (+33.4) and its desulfonated derivative, diplopimarane (+25.8),[21] indicated the same 13*R*,14*S*-configuration.

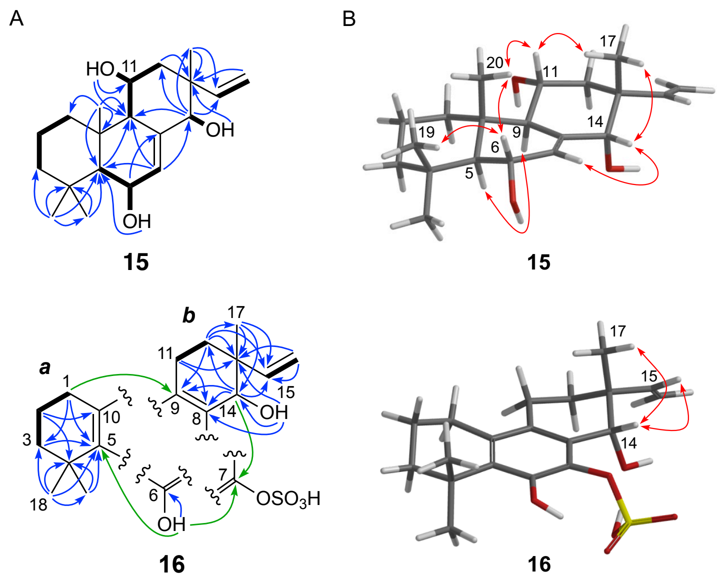

Figure 6. (A) COSY correlations (bold lines) and key HMBCs (arrows) for **15** and **16**. (B) Key NOEs for **15** and **16**.

Inhibitory Effects on RANKL-Induced Formation of Multinuclear Osteoclasts of the Isolated Compounds (1−20). The isolated compounds were evaluated for their inhibitory activities of RANKL-induced osteoclastogenesis and cytotoxicity with RAW264 cells. Cytotoxic activity was assessed at 50 μM, with the compounds having little effect on cell growth (Figure 7A). The enzymatic activity of tartrate-resistant acid phosphatase (TRAP), a marker enzyme of osteoclasts, was examined at 5 μM. RAW264 cells treated with RANKL (50 ng/mL) were incubated in the presence or absence of the compounds (5 μM) for 4 d, and TRAP activity was measured with *p*-nitrophenyl phosphate (Figure 7B). The number of TRAP-positive multinuclear (>3 nuclei) cells was also counted (Figure 7C). In spite of the structural similarities of the tested compounds, only **3**, **7**, and **10** significantly reduced TRAP activity and the number of multinuclear osteoclasts (Figure 8), indicating that these compounds inhibited osteoclast differentiation at 5 μM and their effects were shown to be dose-dependent (Figure 9). Compound **3** was most potent and showed 92% inhibition at a concentration of 0.2 μM. Compared with **3**, **1**, comprising a hydroxy group at C-9, and **2**, lacking the hydroxy group at C-11, were less potent (Figure 10). Similarly, **9**, having a hydroxy group at C-9, was less potent than **10**. In addition, among the two glucosides, **7** was more potent than **6**, which may be due to the influence of the functional groups at C-6 and C-7. These results clearly indicate that the presence of a lactone and glucose moiety are not necessarily related to potency. Owing to the limited availability of these compounds, further examination was carried out using the major constituent **17**, which inhibited formation of TRAP-positive multinuclear cells with IC_{50} of 10.6 μM (Figure 11A). RANKL-induced osteoclastogenic differentiation is associated with upregulation of specific genes. To evaluate if the inhibitory effect of **17** relates to the expression of osteoclastogenic specific genes, total RNA was prepared and analyzed by real-time RT-PCR. Although RANKL (50 ng/mL) induced the expression of *Nfatc1* (Nuclear factor of activated T cells c1; NFATc1), **17** (30 μM) suppressed mRNA expression of the gene by 63% (Figure 11B). This result indicates that compounds **3**, **7**, and **10**, which have the same skeleton structures, may also inhibit formation of TRAP-positive multinuclear cells by suppressing the activation of the NFATc1 signaling pathway.

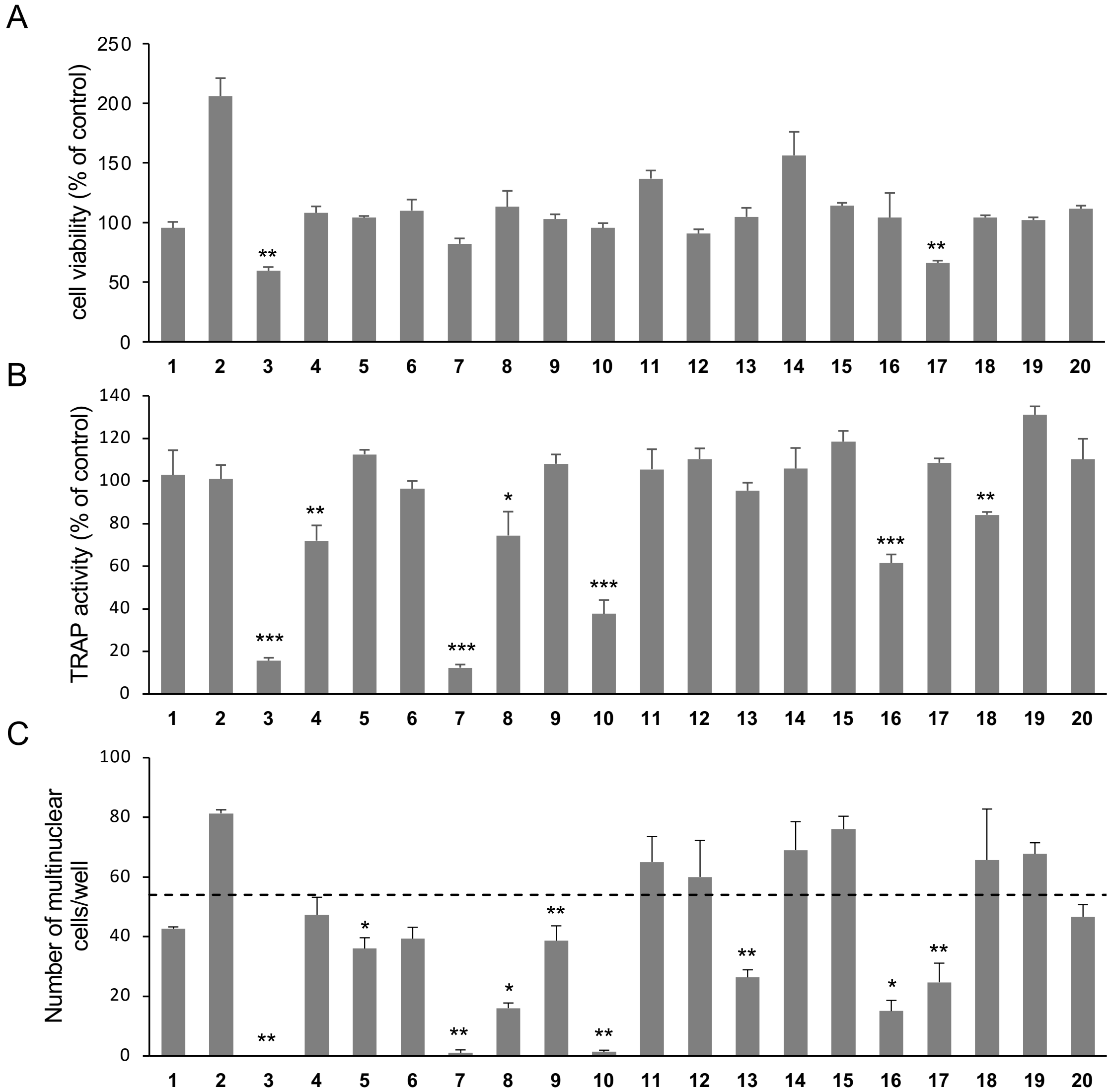

Figure 7. Effects of **1**−**20** on RANKL-induced osteoclast differentiation of RAW 264 cells. (A) RAW 264 cells were treated with RANKL (50 ng/mL) in the presence or absence of **1**−**20** (50 μM) and cultured for 4 d. Cell viability was assessed using the MTT assay. (B) RAW 264 cells were treated with RANKL (50 ng/mL) in the presence or absence of **1**−**20** (5 μM) and cultured for 4 d. TRAP activity was measured with *p*-NPP. (C) RAW 264 cells were treated with RANKL (50 ng/mL) in the presence or absence of **1**−**20** (5 μM) and cultured for 4 d. The cells were stained by TRAP-staining solution, and the number of TRAP-positive multinuclear (>3 nuclei) cells was counted. The dotted line

represents the average number of multinuclear cells in the control. The results are expressed as means ± SD. *p < 0.05, **p < 0.01, and ***p < 0.001 versus the control.

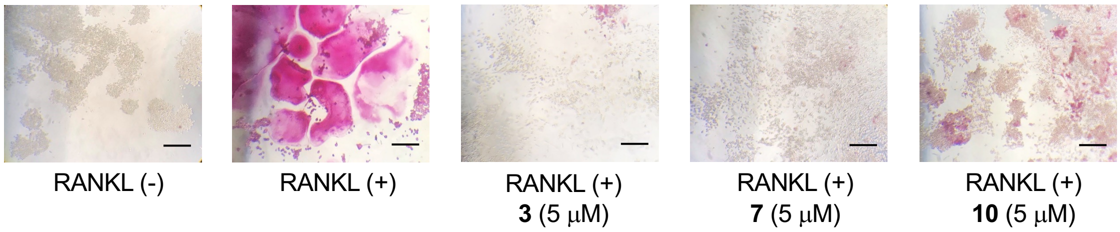

Figure 8. TRAP-stained RAW 264 cells incubated with 50 ng/mL RANKL in the presence or absence of **3**, **7**, and **10** (5 μM). Scale bar represents 200 nm.

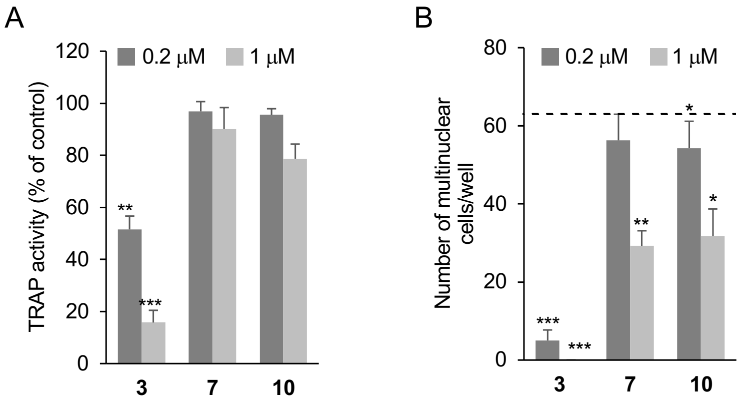

Figure 9. Effects of **3**, **7**, and **10** on RANKL-induced osteoclastogenesis. RAW 264 cells were treated with RANKL (50 ng/mL) in the presence or absence of the compounds at 1 or 0.2 μM for 4 d. TRAP activity (A) and the number of TRAP-positive multinuclear (>3 nuclei) cells (B) were assessed. The dotted line represents the average number of multinuclear cells in the control. The results are expressed as means ± SD. *p < 0.05, **p < 0.01, and ***p < 0.001 versus the control.

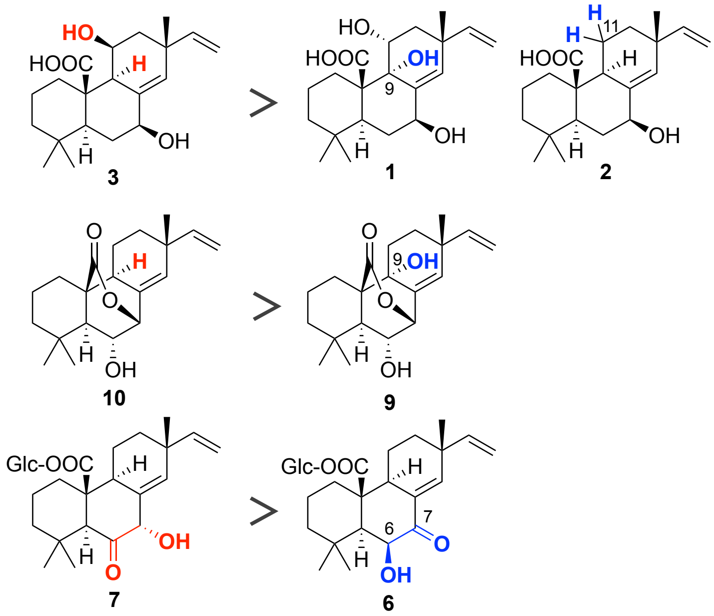

Figure 10. Structure-activity relationship of isolated compounds.

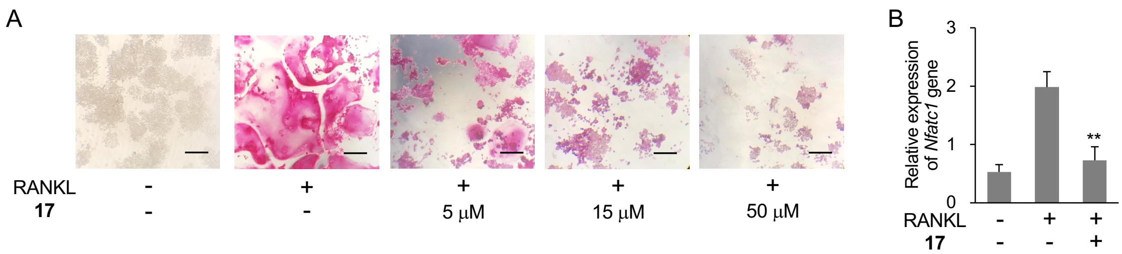

Figure 11. Effects of **17** on RANKL-induced osteoclastogenesis. (A) RAW 264 cells were treated with RANKL (50 ng/mL) in the presence or absence of **17** at the indicated concentrations. After 4 d incubation, the number of TRAP-positive multinuclear (>3 nuclei) cells were counted. Scale bar represents 200 nm. (B) RAW 264 cells treated with RANKL (50 ng/mL) in the presence or absence of **17** (30 μM) were incubated for 24 h. Total RNA was extracted and mRNA expression of *Nfatc1* was evaluated by real-time RT-PCR. The results are expressed as means ± SD. **p < 0.01 versus the control.

EXPERIMENTAL SECTION

General Experimental Procedures. Optical rotations were measured on a JASCO DIP-1000 polarimeter in MeOH, UV spectra on a JASCO V-550 spectrophotometer in MeOH, and ECD spectra on a JASCO J-820 spectropolarimeter in CH_3CN. IR spectra were recorded on a PerkinElmer Frontier FT-IR spectrophotometer. ^1H and ^{13}C NMR spectra were recorded on a Bruker Avance 600 NMR spectrometer in DMSO-d_6, pyridine-d_5, or chloroform-*d*. Chemical shifts were determined with reference to the residual solvent peaks (δ_H 2.49 and δ_C 39.5 for DMSO-d_6; δ_H 7.55 and δ_C 135.5 for pyridine-d_5; δ_H 7.24 for chloroform-*d*). Mass spectra were measured on a Bruker BioTOFQ mass spectrometer, Waters Xevo G2-XS Qtof, or JEOL JMS-700 mass spectrometer. The preparative HPLC system comprised a Waters 515 HPLC pump, Waters 2489 UV/visible detector, and Pantos Unicorder U-228.

Fungal Strain and Culture Conditions. The fungus *A. taichungensis* (IBT 19404), which was isolated from soil in Taiwan, was obtained from the IBT Culture Collection of Fungi in the Technical University of Denmark. The rice medium was made by autoclaving a mixture of rice (5 kg) and water (6 L) before separation into six plastic containers (W17 cm × D22 cm × H9 cm). The fungus suspended in sterilized water was added to the rice medium and cultured at 25°C for 30 d.

Extraction and Isolation. Extraction from the culture was performed with *n*-BuOH. The extract was concentrated and partitioned with H_2O. The *n*-BuOH-soluble fraction was dissolved in 90% MeOH−H_2O and partitioned with *n*-hexane. The aqueous MeOH fraction (50 g) was subjected to ODS column chromatography eluted with a stepwise gradient using 40, 75, 95, and 100% MeOH−H_2O to yield nine fractions (Frs. A1−A9). Fr. A3 was purified by gel filtration HPLC (Asahipak GS-310P, 21.5 × 500 mm; Asahi Chemical Industry Co., Ltd.) with MeOH to afford **17** (640 mg). Fr. A4 (12.6 g) was subjected to SiO_2 column chromatography with 95, 80, 50, and 0% *n*-hexane−EtOAc, 80% CH_2Cl_2−MeOH, and CH_2Cl_2−MeOH–H_2O (6:4:1) to yield 20 fractions (Frs. B1−B20). Frs. B5−B7 were combined (226 mg) and subjected to silica gel column chromatography with a gradient of 50, 33, and 25% *n*-hexane−EtOAc, 90, 85, 80, and 0% CH_2Cl_2−MeOH, and CH_2Cl_2−MeOH−H_2O (6:4:1) to yield 15 fractions (Frs. C1−C15). Fr. C2 was then purified by gel filtration HPLC (Asahipak GS-310P, 21.5 × 500 mm) with MeOH (flow rate, 2 mL/min), and the fraction eluted between 39 and 43 min was purified by HPLC (Develosil C30-UG-5 column, 20 × 250 mm) with 75% MeOH−H_2O to yield **9** (0.68 mg). The fraction eluted between 45 and 55 min was purified by HPLC (Develosil C30-UG-5 column, 20 × 250 mm) with 80% MeOH–H_2O to yield **13** (1.53 mg). Fr. C3 (38.0 mg) was subjected to gel filtration HPLC (Asahipak GS-310P, 21.5 × 500 mm) with MeOH (flow rate, 2 mL/min), and the fraction eluted between 55 and 60 min was purified by C30 HPLC (Develosil C30-UG-5 column, 20 × 250 mm) with 80% MeOH−H_2O followed by HPLC (COSMOSIL πNAP, 10 × 250 mm; Nacalai Tesque Co., Ltd.) with 80% MeOH−H_2O to yield **8** (1.73 mg). Frs. B10 and B11 were combined (970 mg) and subjected to SiO_2 column chromatography eluted by a gradient of 75, 66, 50, 15, and 0% *n*-hexane−EtOAc and MeOH to yield 16 fractions (D1−D16), and Fr. D8 (72.7 mg) was subjected to gel filtration HPLC (Asahipak GS-310P, 21.5 × 500 mm) with MeOH to yield eight fractions (G1−G8). Fr. G1 were purified by HPLC (Develosil C30-UG-5 column, 20 × 250 mm) with 70, 80, and 100% MeOH–H_2O to yield **19** (1.68 mg), **3** (0.54 mg), and **5** (0.71 mg). Fr. G9 was further purified by gel filtration HPLC (Asahipak GS-310P, 21.5 × 500 mm) with MeOH, and the fraction eluted between 53 and 90 min was subjected to ODS column chromatography with a gradient of 60, 70, 80, and 100% MeOH−H_2O to yield Frs. E1−E7. Fr. E3 was further purified by HPLC

(Develosil C30-UG-5 column, 20 × 250 mm) with 70% MeOH−H_2O to yield **1** (3.87 mg), **14** (2.45 mg), and two fractions containing **12** and **15**, respectively. These two fractions were independently purified by HPLC (COSMOSIL πNAP, 10 × 250 mm) with 70% MeOH−H_2O to yield **12** (2.84 mg) and **15** (2.19 mg). Fr. B12 (337.7 mg) was further subjected to NH_2 column chromatography with a stepwise gradient of 0, 50, 100% CH_2Cl_2−CH_3CN and 50% H_2O−CH_3CN to yield 16 fractions (Frs. F1−F16). Fr. F11 was purified by gel filtration HPLC (Asahipak GS-310P, 21.5 × 500 mm) with MeOH to yield seven fractions (Frs. G1−G7). Fr. G6 was subjected to HPLC (Inertsil NH_2, 20 × 250 mm; GL Sciences Inc.) with 95% CH_3CN−H_2O, and the fraction eluted between 95 and 110 min was further purified by gel filtration HPLC (Asahipak GS-310P, 21.5 × 500 mm) with MeOH to yield **7** (1.33 mg). Fr. B14 (2.6 g) was subjected to NH_2 column chromatography with CH_3CN and 97, 90, 80, and 50% CH_3CN−H_2O to yield 15 fractions (Frs. H1−H15). Fr. H11 (101.2 mg) was subjected to gel filtration HPLC (Asahipak GS-310P, 21.5 × 500 mm) with MeOH followed by HPLC (InertSustain phenylhexyl, 20 × 250 mm; GL Sciences Inc.) with a linear gradient 65−75% MeOH−H_2O to yield **16** (10.3 mg). Fr. F13 (110.5 mg) was subjected to diol column chromatography with a gradient of 2, 5, 10, and 100% CH_2Cl_2−MeOH to yield six fractions (Frs. I1−I6). Fr. I3 was purified by HPLC (Develosil C30-UG-5 column, 20 × 250 mm) with 60% MeOH−H_2O to afford **4** (3.85 mg). Fr. H15 (216.4 mg) was purified by gel filtration HPLC (Asahipak GS-310P, 21.5 × 500 mm) with MeOH, and the fraction eluted between 62 and 67 min was further purified by HPLC (Develosil C30-UG-5 column, 20 × 250 mm) eluted with 60% MeOH−H_2O to afford **6** (9.11 mg). Fr. A6 was subjected to SiO_2 column chromatography with 95, 80, 50, and 0% *n*-hexane−EtOAc and 80% CH_2Cl_2−MeOH to yield 15 fractions (Frs. J1−J15). Fr. J5 was purified by HPLC (Develosil C30-UG-5 column, 20 × 250 mm) eluted with 70% MeOH−H_2O to yield **10** (1.44 mg), **11** (3.39 mg), and **20** (0.99 mg). Fr. J15 was purified using the same HPLC column eluted with 75% MeOH−H_2O to yield **2** (2.80 mg).

*Taichunin E (**1**):* $[\alpha]_D^{20}$ +6.1 (*c* 7.6, MeOH); UV (MeOH) λ_{max} (log ε) 282 (3.17) nm; ECD (200 μM, CH_3CN) λ_{max} (Δε) 220 (+0.6); IR (film) ν_{max} 3347, 2922, 2870, 1709, 1636, 1549, 1070, and 969 cm^{-1}; ^1H and ^{13}C NMR data, see Table 1; HRESIMS *m/z* 349.2021 $[M - H]^-$ (calcd for $C_{20}H_{29}O_5$, 349.2020).

*Taichunin F (**2**):* $[\alpha]_D^{20}$ −6.8 (*c* 2.3, MeOH); UV (MeOH) λ_{max} (log ε) 250 (3.9) and 358 (4.0) nm; ECD (400 μM, CH_3CN) λ_{max} (Δε) 220 (+1.13); IR (film) ν_{max} 2951 and 1687 cm^{-1}; ^1H and ^{13}C NMR data, see Table S1; HRESIMS *m/z* 341.2087 $[M + Na]^+$ (calcd for $C_{20}H_{30}O_3Na$, 341.2087).

*Taichunin G (**3**):* $[\alpha]_D^{20}$ +1.8 (*c* 0.16, MeOH); UV (MeOH) λ_{max} (log ε) 234 (4.30) nm; ECD (400 μM, CH_3CN) λ_{max} (Δε) 232 (+0.5); IR (film) ν_{max} 3320, 2923, 2852, 1701, 1595, 1367, 1052, 1033, and 1017 cm^{-1}; ^1H and ^{13}C NMR data, see Table S2; HRESIMS *m/z* 333.2066 $[M - H]^-$ (calcd for $C_{20}H_{29}O_4$, 333.2071).

*Taichunin H (**4**):* $[\alpha]_D^{20}$ +4.6 (*c* 3.2, MeOH); UV (MeOH) λ_{max} (log ε) 250 (4.7) nm; ECD (200 μM, CH_3CN) λ_{max} (Δε) 216 (+2.8) and 248 (−1.9); IR (film) ν_{max} 3388, 2928, 1676, 1606, 1457, 1270, and 1025 cm^{-1}; ^1H and ^{13}C NMR data, see Table S3; HRESIMS *m/z* 355.1881 $[M + Na]^+$ (calcd for $C_{20}H_{28}O_4Na$, 355.1880) and *m/z* 333.2061 $[M + H]^+$ (calcd for $C_{20}H_{29}O_4$, 333.2060).

*Taichunin I (**5**):* $[\alpha]_D^{20}$ +22 (*c* 0.67, MeOH); UV (MeOH) λ_{max} (log ε) 230 (3.3) nm; ECD (200 μM, CH_3CN) λ_{max} (Δε) 222 (+0.5); IR (film) ν_{max} 3358, 2935, 2872, 1687, and 1227 cm^{-1}; ^1H and ^{13}C NMR data, see Table S4; HRESIMS *m/z* 335.2218 $[M - H]^-$ (calcd for $C_{20}H_{31}O_4$, 335.2228).

*Taichunin J (**6**):* $[\alpha]_D^{20}$ −6.6 (*c* 7.6, MeOH); UV (MeOH) λ_{max} (log ε) 250 (5.2) nm; ECD (400 μM, CH_3CN) λ_{max} (Δε) 216 (+3.8) and 248 (−2.5); IR (film) ν_{max} 3366, 2928, 1728, 1611, 1071, 1024, and 992 cm^{-1}; ^1H and ^{13}C NMR data, see Table S5; HRESIMS *m/z* 517.2401 $[M + Na]^+$ (calcd for $C_{26}H_{38}O_9Na$, 517.2408).

Taichunin K (7): $[\alpha]_D^{20}$ −22 (*c* 1.0, MeOH); UV (MeOH) λ_{max} (log ε) 248 (4.4) nm; ECD (200 μM, CH_3CN) λ_{max} (Δε) 216 (+5.3) and 297 (−1.4); IR (film) ν_{max} 3335, 2924, 1733, 1635, and 992 cm^{-1}; ^1H and ^{13}C NMR data, see Table S6; HRESIMS *m/z* 517.2408 $[M + Na]^+$ (calcd for $C_{26}H_{38}O_9Na$, 517.2408).

*Taichunin L (**8**):* $[\alpha]_D^{20}$ +51 (*c* 4.2, MeOH); UV (MeOH) λ_{max} (log ε) 250 (4.7); ECD (400 μM, CH_3CN) λ_{max} (Δε) 208 (+2.7), 242 (−0.8), and 272 (+0.5); IR (film) ν_{max} 3418, 2931, 1767, 1714, 1622, and 1204 cm^{-1}; ^1H and ^{13}C NMR data, see Table S7; HRESIMS *m/z* 347.1863 $[M + H]^+$ (calcd for $C_{20}H_{27}O_5$, 347.1853).

*Taichunin M (**9**):* $[\alpha]_D^{20}$ +28 (*c* 0.50, MeOH); UV (MeOH) λ_{max} (log ε) 275 (3.3) nm; ECD (400 μM, CH_3CN) λ_{max} (Δε) 204 (−21.6); IR (film) ν_{max} 3397, 2928, 1728, 1459, 1371, 1006, and 917 cm^{-1}; ^1H and ^{13}C NMR data, see Table S9; HRESIMS *m/z* 355.1880 $[M + Na]^+$ (calcd for $C_{20}H_{28}O_4Na$, 355.1880).

*Taichunin N (**10**):* $[\alpha]_D^{20}$ −13 (*c* 1.2, MeOH); UV (MeOH) λ_{max} (log ε) 260 (3.1) nm; ECD (400 μM, CH_3CN) λ_{max} (Δε) 204 (−40.1); IR (film) ν_{max} 3445, 2931, and 1729 cm^{-1}; ^1H and ^{13}C NMR data, see Table S10; HRESIMS *m/z* 339.1928 $[M + Na]^+$ (calcd for $C_{20}H_{28}O_3Na$, 339.1931).

*Taichunin O (**11**):* $[\alpha]_D^{20}$ −26 (*c* 2.8, MeOH); UV (MeOH) λ_{max} (log ε) 260 (3.0), nm; ECD (400 μM, CH_3CN) λ_{max} (Δε) 204 (−68.0); IR (film) ν_{max} 3423, 2925, and 1092 cm^{-1}; ^1H and ^{13}C NMR data, see Table S11; HRESIMS *m/z* 347.2233 $[M - H]^-$ (calcd for $C_{21}H_{31}O_4$, 347.2228).

*Taichunin P (**12**):* $[\alpha]_D^{20}$ −43 (*c* 1.7, MeOH); UV (MeOH) λ_{max} (log ε) 238 (5.46) nm; ECD (400 μM, CH_3CN) λ_{max} (Δε) 227 (–2.4), 245 (–2.5), and 273 (+1.1); IR (film) ν_{max} 3342, 2954, 2929, 2869, 1716, 1678, 1302, 1252, 1221, 1177, 1111, and 1024 cm^{-1}; ^1H and ^{13}C NMR data, see Table S12; HRESIMS *m/z* 347.1855 $[M - H]^-$ (calcd for $C_{20}H_{27}O_5$, 347.1864).

*Taichunin Q (**13**):* $[\alpha]_D^{20}$ −79 (*c* 1.3, MeOH); UV (MeOH) λ_{max} (log ε) 248 (4.5) and 310 (4.4) nm; ECD (400 μM, CH_3CN) λ_{max} (Δε) 236 (+17.4) and 307 (–11.5); IR (film) ν_{max} 3432, 2933, 1790, 1678, and 1364 cm^{-1}; ^1H and ^{13}C NMR data, see Table S13; HRESIMS *m/z* 363.1810 $[M + H]^+$ (calcd for $C_{20}H_{27}O_6$, 363.1802).

*Taichunin R (**14**):* $[\alpha]_D^{20}$ −46 (*c* 2.0, MeOH); UV (MeOH) λ_{max} (log ε) 283 (3.2) nm; ECD (400 μM, CH_3CN) λ_{max} (Δε) 214 (–2.8); IR (film) ν_{max} 3365, 2932, 2874, 1774, 1718, 1107, 1024, and 942 cm^{-1}; ^1H and ^{13}C NMR data, see Table S14; HRESIMS *m/z* 363.1812 $[M - H]^-$ (calcd for $C_{20}H_{27}O_6$, 363.1813).

*Taichunin S (**15**):* $[\alpha]_D^{20}$ +20.1 (*c* 1.33, MeOH); UV (MeOH) λ_{max} (log ε) 287 (3.92) nm; IR (film) ν_{max} 3335, 2921, 2852, 1738, 1458, 1414, 1258, 1093, and 1024 cm^{-1}; ^1H and ^{13}C NMR data, see Table S15; HRESIMS *m/z* 343.2260 $[M + Na]^+$ (calcd for $C_{20}H_{32}O_3Na$, 343.2244).

*Taichunin U (**16**):* $[\alpha]_D^{20}$ +33 (*c* 0.43, MeOH); UV (MeOH) λ_{max} (log ε) 288 (4.2) nm; IR (film) ν_{max} 3273, 2925, 2861, 1638, 1428,1260, 1048, and 975 cm^{-1}; ^1H and ^{13}C NMR data, see Table S16; HRESIMS *m/z* 381.1368 $[M - H]^-$ (calcd for $C_{19}H_{25}O_6S$, 381.1377).

Conformational Analyses and ECD Calculations. These experiments were performed as previously described[22] using Spartan'18 instead of Spartan'16. ECD calculations were performed at the BHandHLYP/TZVP level.

Absolute Configuration of Glucose in 6 and 7. Compounds **6** and **7** (each 0.1 mg) were hydrolyzed with 0.5 M HCl (0.1 mL) at 60°C for 1 h. After evaporation, the residue was dissolved in pyridine (0.1 mL) and reacted with L-cysteine methyl ester (0.5 mg) at 60 °C. After 1 h, isothiocyanate (0.5 mg) was added to the solution, and the reaction mixture was kept at 60 °C for 1 h. A portion (2 μL) of the solution was subjected to analysis by HPLC [Cosmosil 5C18-AR-II, 4.6 × 250 mm; solvent, CH_3CN−0.2% trifluoroacetic acid in H_2O (25:75); flow rate, 1 mL/min; detector, UV (254 nm)]. The retention times of the standard D- and L-glucose derivatives were 13.5 and 12.4 min, respectively.

Acetylation of 7. Compound **7** (80 μg) was dissolved in 50 μL of pyridine and mixed with 50 μL of acetic anhydride for 12 h at room temperature with stirring. Then, 100 μL of cold water was added to the reaction mixture, and the solution was concentrated and partitioned between water and EtOAc. The EtOAc layer was evaporated, and the NMR spectrum of the product (**7a**) was measured.

7a: ^{1}H NMR (chloroform-*d*) δ_H 5.84 (s, H-14), 5.69 (dd, *J* = 17.4, 10.6 Hz, H-15), 5.52 (d, *J* = 8.4 Hz, H-1’), 5.31 (s, H-7), 5.19 (t, *J* = 9.4 Hz, H-3’), 5.08 (dd, *J* = 9.4, 8.4 Hz, H-2’), 5.03 (t, *J* = 9.4 Hz, H-4’), 4.91 (d, *J* = 10.6 Hz, H-16a), 4.87 (d, *J* = 17.4 Hz, H-16b), 4.21 (dd, *J* = 12.4, 5.7 Hz, H-6’a), 3.97 (dd, *J* = 12.4, 1.9 Hz, H-6’b), 3.74 (m, H-5’), 2.54 (dd, *J* = 19.7, 12.3 Hz, H-9), 2.07 (s, H_3-Ac), 2.02 (s, H_3-Ac), 2.01 (s, H_3-Ac), 2.00 (s, H_3-Ac), 1.99 (s, H_3-Ac), 0.98 (s, H_3-18), and 0.94 (s, H_3-19); ESIMS *m/z* 727 [M + Na]$^+$.

Reduction of 8. To 0.5 mg of **8** in 100 μL of MeOH, 0.22 mg of $NaBH_4$ was added, and the mixture was stirred at 0 °C for 1 h and allowed to stand at 27 °C for 1 h. The solution was dried, and the CH_2Cl_2-soluble layer was afforded as a reductant of **8** (**8a**).

The relative configuration of C-7 of **8a** remained undetermined due to the small amount obtained.

8a: ^{1}H and ^{13}C NMR data, see Table S8; FABMS *m/z* 383.5 [M + Cl]$^-$.

TRAP Activity. TRAP activity was measured as previously described.[5]

Multinuclear Osteoclast Formation. Multinuclear osteoclasts were counted as previously described. [5]

Cytotoxicity Assay. RAW264 cells were cultured in the presence of the test compounds in a humidified atmosphere containing 5% CO_2 at 37°C for 4 d. Cell viability was tested using the MTT assay as previously described.[23]

Real-time RT-PCR Analysis. RAW 264 cells seeded on a 6-well plate (2.7×10^4 cells/well) were treated with sRANKL (50 ng/mL) and **17** (30 μM) and incubated for 24 h. RNA extraction and real-time RT-PCR analysis were conducted as previously described.[9]

ASSOCIATED CONTENT

Supporting Information

The Supporting Information is available free of charge at https://pubs.acs.org/doi/10.1021/acs.jnatprod.xxxxxxx.

NMR spectra of **1**−**16**, **7a**, and **8a**; NMR data of **2**−**16** and **8a** (PDF)

AUTHOR INFORMATION

Corresponding Author

Sachiko Tsukamoto – *Department of Natural Medicines, Graduate School of Pharmaceutical Sciences, Kumamoto University, 5-1 Oe-honmachi, Kumamoto*

862-0973, Japan; http://orcid.org/0000-0002-7993-381X; E-mail: sachiko@kumamoto-u.ac.jp

Authors

Ahmed H. H. El-Desoky – *Department of Natural Medicines, Graduate School of Pharmaceutical Sciences, Kumamoto University, 5-1 Oe-honmachi, Kumamoto 862-0973, Japan; Pharmaceutical Industries Research Division, Pharmacognosy Department, National Research Centre, 33 El Bohouth St. (Former El Tahrir St.), Dokki, P.O. 12622, Giza, Egypt.*

Natsumi Inada – *Department of Natural Medicines, Graduate School of Pharmaceutical Sciences, Kumamoto University, 5-1 Oe-honmachi, Kumamoto 862-0973, Japan.*

Yuka Maeyama – *Department of Natural Medicines, Graduate School of Pharmaceutical Sciences, Kumamoto University, 5-1 Oe-honmachi, Kumamoto 862-0973, Japan.*

Hikaru Kato – *Department of Natural Medicines, Graduate School of Pharmaceutical Sciences, Kumamoto University, 5-1 Oe-honmachi, Kumamoto 862-0973, Japan.* http://orcid.org/0000-0001-9551-831X.

Yuki Hitora – *Department of Natural Medicines, Graduate School of Pharmaceutical Sciences, Kumamoto University, 5-1 Oe-honmachi, Kumamoto 862-0973, Japan.* http://orcid.org/0000-0003-4271-2543.

Momona Sebe – *Department of Natural Medicines, Graduate School of Pharmaceutical Sciences, Kumamoto University, 5-1 Oe-honmachi, Kumamoto 862-0973, Japan.*

Mika Nagaki – *Department of Natural Medicines, Graduate School of Pharmaceutical Sciences, Kumamoto University, 5-1 Oe-honmachi, Kumamoto 862-0973, Japan.*

Aika Kai – *Department of Natural Medicines, Graduate School of Pharmaceutical Sciences, Kumamoto University, 5-1 Oe-honmachi, Kumamoto 862-0973, Japan.*

Keisuke Eguchi – *Department of Natural Medicines, Graduate School of Pharmaceutical Sciences, Kumamoto University, 5-1 Oe-honmachi, Kumamoto 862-0973, Japan.*

Tomoaki Inazami – *Department of Pharmaceutical Biochemistry, Graduate School of Pharmaceutical Sciences, Kumamoto University, 5-1 Oe-honmachi, Kumamoto 862-0973, Japan.*

Yukihiko Sugimoto – *Department of Pharmaceutical Biochemistry, Graduate School of Pharmaceutical Sciences, Kumamoto University, 5-1 Oe-honmachi, Kumamoto 862-0973, Japan.*

Jens C. Frisvad – *Section for Synthetic Biology, Department of Biotechnology and Biomedicine, Soltofts Plads Building 221, Technical University of Denmark, 2800 Kongens Lyngby, Denmark.*

Robert M. Williams – *Department of Chemistry, Colorado State University, 1301 Center Avenue, Fort Collins, CO 80523, USA.* http://orcid.org/0000-0001-9063-1284.

Author Contributions

A.H.H.E., N.I., and Y.M. contributed equally to this work.

Notes

The authors declare that they have no competing financial interests.

ACKNOWLEDGMENT

This work was supported by JSPS KAKENHI Grant Numbers JP20H03396 (S.T.), JP18K06719 (H.K.), JP20K16026 (Y.H.), and JP20K22710 (A.H.H.E.), and Useful and Unique Natural Products for Drug Discovery and Development (UpRod), Program for Building Regional Innovation Ecosystems at Kumamoto University, Japan.

REFERENCES and NOTES

[1] Boyle, W. J.; Simonet, W. S.; Lacey, D. L. *Nature* **2003**, *423*, 337−342.

[2] Takayanagi, H. *Nat. Rev. Immunol.* **2007**, *7*, 292−304.

[3] Boyce, B. F. *J. Dent. Res.* **2013**, *92*, 860−867.

[4] Rachner, T. D.; Khosla, S.; Hofbauer, L. C. *Lancet* **2011**, *377*, 1276−1287.

[5] Tsukamoto, S.; Takeuchi, T.; Kawabata, T.; Kato, H.; Yamakuma, M.; Matsuo, K.; El-Desoky, A. H.; Losung, F.; Mangindaan, R. E.; Voogd, N. J. D.; Arata, Y.; Yokosawa, H. *Bioorg. Med. Chem. Lett.* **2014**, *24*, 5315−5317.

[6] El-Desoky, A. H.; Kato, H.; Angkouw, E. D.; Mangindaan, R. E. P.; Voogd, N. J. D.; Tsukamoto, S. *J. Nat. Prod.* **2016**, *79*, 1922−1928.

[7] El-Desoky, A. H.; Kato, H.; Kagiyama, I.; Hitora, Y.; Losung, F.; Mangindaan, R. E. P.; Voogd, N. J. D.; Tsukamoto, S. *J. Nat. Prod.* **2017**, *80*, 90−95.

[8] El-Beih, A. A.; El-Desoky, A. H.; Al-Hammady, M. A.; Elshamy, A. I.; Hegazy, M.-E. F.; Kato, H.; Tsukamoto, S. *Fitoterapia* **2018**, *128*, 43−49.

[9] Kato, H.; Kai, A.; Kawabata, T.; Sunderhaus, J. D.; Mcafoos, T. J.; Finefield, J. M.;

Sugimoto, Y.; Williams, R. M.; Tsukamoto, S. *Bioorg. Med. Chem. Lett.* **2017**, *27*, 4975−4978.

[10] Kato, H.; Yoshida, T.; Tokue, T.; Nojiri, Y.; Hirota, H.; Ohta, T.; Williams, R. M.; Tsukamoto, S. *Angew. Chem., Int. Ed.* **2007**, *46*, 2254–2256.

[11] Greshock, T. J.; Grubbs A. W.; Jiao, P.; Wicklow, D. T.; Gloer, J. B.; Williams, R. M. *Angew. Chem., Int. Ed.* **2008**, *47*, 3573–3577.

[12] Reveglia, P.; Cimmino, A.; Masi, M.; Nocera, P.; Berova, N.; Ellestad, G.; Evidente, A. *Chirality* **2018**, *30*, 1115–1134.

[13] Evidente, A.; Sparapano, L.; Motta, A.; Giordano, F.; Fierro, O.; Frisullo, S. *Phytochemistry* **1996**, *42*, 1541–1546.

[14] Evidente, A.; Sparapano, L.; Fierro, O.; Bruno, G.; Giordano, F.; Motta, A. *Phytochemistry* **1997**, *45*, 705−713.

[15] Kagiyama, I.; Kato, H.; Nehira, T.; Frisvad, J. C.; Sherman, D. H.; Williams, R. M.; Tsukamoto, S. *Angew. Chem., Int. Ed.* **2016**, *55*, 1128−1132.

[16] Klas, K.; Kato, H.; Frisvad, J. C.; Yu, F.; Newmister, S.; Fraley, A.; Sherman, D. H.; Tsukamoto, S.; Williams, R. M. *Nat. Prod. Rep.* **2018**, *35*, 532–558.

[17] Kato, H.; Sebe, M.; Nagaki, M.; Eguchi, K.; Kagiyama, I.; Hitora, Y.; Frisvad, J. C.; Williams, R. M.; Tsukamoto, S. *J. Nat. Prod.* **2019**, *82*, 1377−1381.

[18] Guo, Z. K.; Yan, T.; Guo, Y.; Song, Y. C.; Jiao, R. H.; Tan, R. X.; Ge, H. M. *J. Nat. Prod.* **2012**, *75*, 15−21.

[19] Bohlmann, F.; Lonitz, M. *Chem. Ber.* **1978**, *111*, 843−852.

[20] Tanaka, T.; Nakashima, T.; Ueda, T.; Tomii, K.; Kouno, I. *Chem. Pharm. Bull.* **2007**, *55*, 899−901.

[21] Andolfi, A.; Maddau, L.; Basso, S.; Linaldeddu, B. T.; Cimmino, A.; Scanu, B.;

Deidda, A.; Tuzi, A.; Evidente, A. *J. Nat. Prod.* **2014**, *77*, 2352−2360.

[22] Torii, M.; Kato, H.; Hitora, Y.; Angkouw, E. D.; Mangindaan, R. E. P.; Voogd, N. J. D.; Tsukamoto, S. *J. Nat. Prod.* **2017**, *80*, 2536−2541.

[23] Afifi, A. H.; El-Desoky, A. H.; Kato, H.; Mangindaan, R. E. P.; de Voogd, N. J.; Ammar, N. M.; Hifnawy, M. S.; Tsukamoto, S. *Tetrahedron Lett*. **2016**, *57*, 1285−1288.

Table of Contents/Abstract Graphic